Pedley, T.J., Hill, N.A., and Kessler, J.O. (1988) *The growth of bioconvection patterns in a uniform suspension of gyrotactic micro-organisms*. Journal of Fluid Mechanics, 195 . pp. 223-237. ISSN 0022-1120 (doi:10.1017/S0022112088002393)

Copyright © 1988 Cambridge University Press

A copy can be downloaded for personal non-commercial research or study, without prior permission or charge

Content must not be changed in any way or reproduced in any format or medium without the formal permission of the copyright holder(s)

When referring to this work, full bibliographic details must be given

http://eprints.gla.ac.uk/88746/

Deposited on: 19 December 2013

Enlighten – Research publications by members of the University of Glasgow
http://eprints.gla.ac.uk

J. Fluid Mech. (1988), *vol.* 195, *pp.* 223–237
Printed in Great Britain

The growth of bioconvection patterns in a uniform suspension of gyrotactic micro-organisms

By T. J. PEDLEY,† N. A. HILL† AND J. O. KESSLER‡

† Department of Applied Mathematics and Theoretical Physics, University of Cambridge, Silver Street, Cambridge CB3 9EW, UK

‡ Department of Physics, University of Arizona, Tucson, AZ 85721, USA

(Received 6 October 1987 and in revised form 6 April 1988)

'Bioconvection' is the name given to pattern-forming convective motions set up in suspensions of swimming micro-organisms. 'Gyrotaxis' describes the way the swimming is guided through a balance between the physical torques generated by viscous drag and by gravity operating on an asymmetric distribution of mass within the organism. When the organisms are heavier towards the rear, gyrotaxis turns them so that they swim towards regions of most rapid downflow. The presence of gyrotaxis means that bioconvective instability can develop from an initially uniform suspension, without an unstable density stratification. In this paper a continuum model for suspensions of gyrotactic micro-organisms is proposed and discussed; in particular, account is taken of the fact that the organisms of interest are non-spherical, so that their orientation is influenced by the strain rate in the ambient flow as well as the vorticity. This model is used to analyse the linear instability of a uniform suspension. It is shown that the suspension is unstable if the disturbance wavenumber is less than a critical value which, together with the wavenumber of the most rapidly growing disturbance, is calculated explicitly. The subsequent convection pattern is predicted to be three-dimensional (i.e. with variation in the vertical as well as the horizontal direction) if the cells are sufficiently elongated. Numerical results are given for suspensions of a particular algal species (*Chlamydomonas nivalis*); the predicted wavelength of the most rapidly growing disturbance is 5–6 times larger than the wavelength of steady-state patterns observed in experiments. The main reasons for the difference are probably that the analysis describes the onset of convection, not the final, nonlinear steady state, and that the experimental fluid layer has finite depth.

1. Introduction

The phenomenon of 'bioconvection' has been familiar for some time (Loeffer & Mefferd 1952; Platt 1961; Winet & Jahn 1972). Cellular streaming patterns are observed in liquid suspensions of swimming micro-organisms (*Tetrahymena*, for example), in which bulk fluid motions occur, downwards in regions where high concentrations of micro-organisms develop, and upwards in regions of low concentration. The type of pattern depends on quantities such as the suspension depth and the concentration and motility of the organisms. A convincing model was presented and analysed by Childress, Levandowsky & Spiegel (1975) and Levandowsky *et al.* (1975), in which the source of the patterns was attributed to a hydrodynamic instability analogous to that causing Rayleigh–Bénard convection. The organisms in question tend to swim vertically upwards, a process that may be

described as 'negative geotaxis'. Because they are denser than the suspending water, their up-swimming causes the upper regions of the suspension to become denser than the lower, and when the gradient in volume concentration becomes sufficiently large an overturning convection occurs. The critical concentration gradient is represented by a critical Rayleigh number, as in Rayleigh–Bénard convection. The 'cell diffusivity' that appears in the Rayleigh number comes from modelling random aspects of cells' swimming behaviour; a model in which this was ignored, and the instability likened to viscous Rayleigh–Taylor instability, has previously been presented by Plesset & Winet (1974).

Recently Kessler (1984, 1985*a*, *b*, 1986*a*, *b*) has shown that many micro-organisms, such as members of the genera *Dunaliella*, *Chlamydomonas*, *Volvox* and *Peridinium* swim upwards in still water, as a consequence of their inhomogeneous mass distribution. The centre of mass of a typical up-swimming organism is displaced from the centre of buoyancy in a direction opposite to the swimming direction: in other words the cell is bottom-heavy. When such organisms swim in a flow field with a horizontal component of vorticity, for example, they experience a viscous torque which is countered by the gravitational torque so that they tend to swim at an angle to the vertical. This determination of swimming direction by a *balance* between viscous and gravitational torques is termed 'gyrotaxis'. The term includes 'rheotaxis', used to describe the tendency of very elongated micro-organisms (spermatozoa in particular) to become aligned with the flow direction in a shear flow. Coupled with their positive geotaxis (they are head-heavy and therefore swim downwards), rheotaxis causes spermatozoa to tend to swim upstream, in the lower half of a flow between horizontal microscope slides or in a horizontal tube (Roberts 1970). Winet, Bernstein & Head (1984) demonstrated that rheotaxis in spermatozoa is virtually unaffected when the flow is directed vertically instead of horizontally (at one particular flow rate).

Gyrotaxis causes bottom-heavy cells to be concentrated in regions of downflow and away from regions of upflow. The regions of downflow thus become denser than their surroundings, and the velocity difference between downflow and upflow is enhanced. This is a mechanism for the spontaneous growth of concentration fluctuations, which can presumably develop into observable convection patterns, even in the absence of a mean vertical concentration gradient. Kessler (1986*a*) has demonstrated such convection patterns experimentally in initially well-stirred suspensions; ultimately, tall plumes of downflow are observed, spaced regularly across the flow chamber.

The purpose of the present paper is to provide a quantitative model for the onset of this type of convection, from which predictions of initial plume spacing can be derived and compared with observation. A preliminary model was given by Kessler (1986*b*), but he restricted his analysis by (*a*) assuming that the micro-organisms are spherical, so that the only feature of the velocity field that influences their orientation is the (horizontal component of the) vorticity, not the rate of strain; (*b*) considering only disturbances that are independent of the vertical component and are axisymmetric; (*c*) neglecting the inertia of the fluid. Here we relax all those restrictions, and are able to make predictions that differ significantly from Kessler's.

The analysis is based on a continuum model of the suspension, and in §2 we describe that model in detail; in particular we improve on previous derivations by (*a*) justifying the neglect of the effect of the cells, including their swimming motions, on the bulk fluid stress (neglect of the 'stresslet' term), and (*b*) utilizing our recent analysis of the orientation of spheroidal cells in a general flow (Pedley & Kessler

1987, hereafter referred to as P & K). Apart from the vital inclusion of gyrotaxis, the continuum model is very similar to that used by Childress *et al.* (1975). In §3, a linear stability analysis of an initially uniform suspension is presented, and results are obtained both generally and in particular limits. Quantitative comparison with experiment, and further discussion, is given in §4.

2. The continuum model

The model is based on the assumption that the lengthscale of the bulk motions and concentration distribution is large compared with cell diameter and typical cell spacing. These quantities have approximate values of 10^{-3} and 10^{-2} cm respectively (see tables 1 and 2 in §4 for numerical values of these and other quantities), while the observed and predicted lengthscales of convection patterns are in the range 0.2–2.0 cm, so we can, as a first approximation, neglect the microstructure. We also neglect inertia in all aspects of the dynamics of the cells' motion relative to the fluid. We suppose that a volume element δV contains $n(\boldsymbol{x}, t)\,\delta V$ identical cells of volume v and density $\rho + \Delta\rho$, where ρ is the uniform density of water and $\Delta\rho \ll \rho$ (table 1). The suspension is taken to be dilute, i.e. we assume the volume concentration $nv \ll 1$. We define $\boldsymbol{u}(\boldsymbol{x}, t)$ as the mass average velocity of all material in δV, and the average swimming speed of the cells in δV, relative to the bulk, is taken to be $V_c \boldsymbol{p}$. Here V_c is assumed constant, while $\boldsymbol{p}(\boldsymbol{x}, t)$ is a unit vector in the swimming direction. We assume that water and cells are incompressible, so that conservation of volume gives

$$\operatorname{div} \boldsymbol{u} = 0. \tag{2.1}$$

In the momentum equation for the suspension we make the Boussinesq approximation, that the variations in density consequent upon concentration fluctuations are negligible in the inertia terms (valid since $nv\Delta\rho/\rho \ll 1$), but important in the buoyancy force term that drives the fluid motion. This force, for fluid volume δV, is equal to the gravitational acceleration $\boldsymbol{g}$ times $nv\Delta\rho\,\delta V$, the excess mass of the cells occupying δV. One might prefer to think of the suspensions as consisting of two distinct phases, water and cells, in which case the effect exerted on the water by the cells in δV is the sum of $n\,\delta V$ Stokeslets, each of strength $\boldsymbol{g}v\Delta\rho$. This is equal and opposite to the force exerted by the water on the cells (apart from the hydrostatic upthrust), and equal to the force exerted by gravity on the cells, so the net force on the suspension is the same as before. The equation of motion for the cells would be needed to investigate their sedimentation relative to the water, but a typical sedimentation velocity is much smaller than the swimming speed (table 2), justifying our assumption that the cells swim with an independently known relative velocity. In the absence of any additional forces, the momentum equation for the suspension is

$$\rho \frac{\mathrm{D}\boldsymbol{u}}{\mathrm{D}t} = -\nabla p_e + nv\Delta\rho\,\boldsymbol{g} + \mu\nabla^2\boldsymbol{u}, \tag{2.2}$$

where $\mathrm{D}/\mathrm{D}t$ is the convective derivative, p_e is the pressure excess above hydrostatic (at density ρ), and μ is the dynamic viscosity of the suspension, assumed to be approximately the same as that of water.

However, the effect of the cells on the fluid motion is not confined to the buoyancy force; in addition to a force, each cell exerts a couple, $\boldsymbol{L}$, on the fluid, as a result of the gravitational couple on the cell. Thus, in addition to a Stokeslet strength, each cell possesses a couplet and a stresslet strength as well (and higher-order singularities). The aggregate of the couplets and stresslets makes a contribution to the bulk stress of the suspension. Batchelor (1970) shows that the additional stress

in volume δV of a suspension of inert, force-free, non-spherical particles is given by

$$\Sigma_{ij}^{(\mathrm{p})} = \frac{1}{\delta V} \Sigma \{4\pi\mu C_{ijkl} e_{kl} + \tfrac{1}{2}(B_{ijk} + \epsilon_{ijk}) L_k\}, \tag{2.3}$$

where e_{kl} is the bulk rate-of-strain tensor, the summation is over all particles in δV, and B_{ijk} and C_{ijkl} are tensors whose components depend on the particle geometry. When there is a relative velocity $\boldsymbol{u}_{\mathrm{rel}}$ between particle and fluid, as here, there may be an additional contribution to $\Sigma_{ij}^{(\mathrm{p})}$ of the form $Q'_{ijk} u_{\mathrm{rel}_k}$, where the components of Q'_{ijk} are the same, but reordered, as those of the tensor Q_{ijk} giving the force on a particle caused by bulk rate of strain (as opposed to relative velocity or angular velocity), i.e. $Q_{ijk} e_{jk}$ (Hinch 1972). However, we assume that the cells have a symmetry such that they experience no force in a pure straining motion (e.g. they may be spheroidal); hence $Q'_{ijk} \equiv 0$, and (2.3) gives the complete (inert) particle stresslet contribution to the stress. This contribution can be neglected in the momentum equation if its divergence is small compared with ρ times the other terms in (2.2). Batchelor (1970) gave expressions for the components of B_{ijk} and C_{ijkl} in the case of rigid, ellipsoidal particles. These expressions show that $C_{ijkl} = O(v)$ while $B_{ijk} = O(1)$. Thus the first term on the right-hand side of (2.3) has order of magnitude $n\mu v e_{kl}$ which is much less than μe_{kl} (which yields the last term of (2.2)), since $nv \ll 1$. Moreover, the divergence of the second term on the right of (2.3) has order of magnitude nL/r, where L is the magnitude of $\boldsymbol{L}$ and r is a macroscopic lengthscale for the flow. Now, since a cell's motion relative to the fluid is inertia-free, the couple exerted by a cell on the fluid is the same as the couple exerted by gravity on the cell, i.e.

$$\boldsymbol{L} = \boldsymbol{h} \times \rho v \boldsymbol{g}, \tag{2.4}$$

where $\boldsymbol{h}$ is the displacement of the centre of mass of the cell from the centre of buoyancy. Hence $nL/r \sim nh\rho vg/r$, while ρ times the buoyancy force term in (2.2) has order of magnitude $n\Delta\rho vg$. Thus the former is negligible if $h/r \ll \Delta\rho/\rho$, or, using the data from table 1, $r \gg 2\ \mu\mathrm{m}$; we assume this to be the case.

An estimate of the further contribution made to the stresslet strength of a cell by its active swimming motions can be made if we know something of how the cell moves. The algal cells of interest here swim by means of a low-Reynolds-number breast-stroke, using two flagella mounted at the front of the body, which is assumed to be spheroidal. Assuming that most of the drag on the cell, as it swims forward with speed V_{c}, comes from the body surface, the order of magnitude of this quantity can be estimated to be $\mu d V_{\mathrm{c}}$, where d is a typical cell diameter. Each flagellum therefore exerts a thrust of half this magnitude. Assuming also that the points of application of the thrust forces are located at a distance of order d ahead (and to the side) of the centre of the body, the stresslet strength of each cell is of order $\mu d^2 V_{\mathrm{c}}$, and thus the stresslet strength per unit volume of cell is $\mu V_{\mathrm{c}}/d$ (assuming $v \sim d^3$). Per unit volume of suspension, therefore, the contribution to $\Sigma_{ij}^{(\mathrm{p})}$ is of order $nv\mu V_{\mathrm{c}}/d$. To be negligible, this must be small compared with $\mu e_{kl} \sim \mu U/r$, where U is a bulk velocity scale, i.e.

$$\frac{U}{r} \gg nv \frac{V_{\mathrm{c}}}{d} \sim 5 \times 10^{-3}\ \mathrm{s}^{-1},$$

which is a smaller strain rate than those commonly seen in bioconvection (Kessler 1985*b*), but not very much smaller. Thus its neglect is justified as a first approximation, but the continuum model should eventually incorporate a volume concentration of active stresslets.

Another feature of real micro-organisms that is neglected here is the fact that almost all of them rotate when swimming as a result of some asymmetry in their geometry or flagellar motions. The axis of such autorotation is generally parallel to the swimming direction, and therefore does not influence it (P & K), and any particular genus of micro-organism has a particular sense of rotation (Rüffer & Nultsch 1985). The net couple exerted on a volume element of the continuum by autorotating micro-organisms is of course zero, and the effect on the suspension is to introduce a volume distribution of 'couplets' (Batchelor 1970), analogous to the stresslets discussed above, and negligible for the same reasons.

The other conservation equation required in the continuum model is that representing conservation of cells. This can be written

$$\frac{\partial n}{\partial t} = -\operatorname{div} \boldsymbol{j}, \tag{2.5}$$

where $\boldsymbol{j}(\boldsymbol{x}, t) \cdot \delta \boldsymbol{S}$ is the net flux of cells across the surface element $\delta \boldsymbol{S}$ at $\boldsymbol{x}$. There will be three contributions to $\boldsymbol{j}$: one due to advection by the bulk flow, one due to the cells' swimming, and a third $\boldsymbol{j}_D$ to represent all the random aspects of cell movement, such as translational Brownian motion, cell–cell interactions and the fact that the cells in a volume element δV have a distribution of swimming velocities, of which only the mean is $V_c \boldsymbol{p}$ (for reasons of either intrinsic variability or rotational Brownian motion). Thus we can write

$$\boldsymbol{j} = n(\boldsymbol{u} + V_c \boldsymbol{p}) + \boldsymbol{j}_D, \tag{2.6}$$

and it remains to evaluate $\boldsymbol{j}_D$. Here we follow Childress *et al.* (1975), and represent all random motions by a diffusive process, which we assume to be isotropic:

$$j_{D_i} = -D_{ij} \frac{\partial n}{\partial x_j} = -D \frac{\partial n}{\partial x_i}, \tag{2.7}$$

where D is the isotropic diffusivity. In fact Childress *et al.* took the tensor D_{ij} to be orthotropic, with different diffusivities for vertical and horizontal diffusion, but since we have no means of estimating the different values, we assume them to be the same. Kessler (1985*b*, 1986*a*) has made two independent estimates of the value of D, based on assumptions about cell–cell collisions and about random cell swimming respectively, and they were both in the range 5×10^{-5} to 5×10^{-4} cm^2 s^{-1}. However, in general D_{ij} is likely to depend on n, since the time between cell–cell collisions will decrease as the concentration increases, and on the flow field through its effect on the gyrotactic process: the more rapidly a cell's swimming direction $\boldsymbol{p}$ is reoriented by gyrotaxis, the narrower will be the probability density function of $\boldsymbol{p}$ about its mean value (this effect is particularly marked for long, narrow micro-organisms such as spermatozoa; see Winet *et al.* 1984). Future development of the present work will require a more rigorous investigation of $\boldsymbol{j}_D$.

The final component of the model is an equation for the average swimming direction $\boldsymbol{p}$. We now assume that all cells occupying a volume element δV swim with the *same* velocity $V_c \boldsymbol{p}$. We also assume that the (identical) cells are spheroidal, with axis of symmetry parallel to $\boldsymbol{p}$, and with centre of mass displaced by $-h\boldsymbol{p}$ from the geometric centre of the cell (thus we ignore, for example, the effect of the flagella themselves on a cell's orientation). We can therefore use the theory of P & K to determine $\boldsymbol{p}(\boldsymbol{x}, t)$ in terms of the vorticity $\boldsymbol{\omega}(\boldsymbol{x}, t)$ and the rate-of-strain tensor $e_{ij}(\boldsymbol{x}, t)$. The vector $\boldsymbol{p}$ is specified by Euler angles θ, ϕ referred to axes $C123$ through

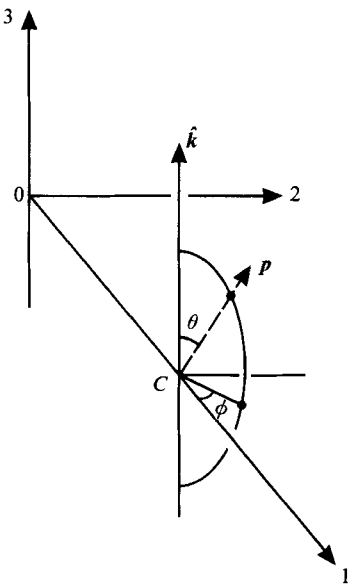

FIGURE 1. Cartesian axes and Euler angles; the curve represents a semicircle in the vertical plane containing $\hat{\boldsymbol{k}}$ and $\boldsymbol{p}$. The micro-organism is depicted only through its symmetry axis, $\boldsymbol{p}$.

the geometric centre, C, of the cell and parallel to the laboratory, Cartesian axes (figure 1):

$$\boldsymbol{p} = (\sin\theta\cos\phi,\ \sin\theta\sin\phi,\ \cos\theta). \tag{2.8}$$

It was shown in P & K that the balance between gravitational and viscous torques leads to the following equations from which θ and ϕ can be determined:

$$\omega_2\cos\phi-\omega_1\sin\phi+\alpha_0\{\sin 2\theta(e_{11}\cos^2\phi+2e_{12}\sin\phi\cos\phi + e_{22}\sin^2\phi-e_{33})+2\cos 2\theta(e_{13}\cos\phi+e_{23}\sin\phi)\} = B^{-1}\sin\theta, \tag{2.9}$$

$$-\omega_1\cos\theta\cos\phi-\omega_2\cos\theta\sin\phi+\omega_3\sin\theta+\alpha_0\{\sin\theta(-e_{11}\sin 2\phi+2e_{12}\cos 2\phi + e_{22}\sin 2\phi)+2\cos\theta(-e_{13}\sin\phi+e_{23}\cos\phi)\} = 0, \tag{2.10}$$

where

$$\alpha_0 = (a^2-b^2)/(a^2+b^2), \tag{2.11}$$

a and b being the semi-major and -minor axes of the spheroidal cell, so α_0 represents the cell eccentricity ($0 \leqslant \alpha_0 < 1$), and B is the 'gyrotactic orientation parameter'

$$B = \mu\alpha_\perp/2h\rho g \tag{2.12}$$

with $\alpha_\perp$ being a dimensionless constant relating viscous torque to the relative angular velocity of the cell. Also given in P & K were the conditions for the local equilibrium orientation given by (2.9) and (2.10) to be stable; i.e. for the cells not to tumble. In all cases considered in subsequent sections these conditions are satisfied, because θ, representing the departure of $\boldsymbol{p}$ from the vertical, is small; we therefore do not reproduce the conditions here. The continuum model is now complete.

3. Linear stability theory

The basic state whose stability will be examined is that of a uniform suspension of cells, with number density n_0, in an infinite body of fluid. All cells are swimming

vertically upwards, but because of the infinite extent this does not change the concentration or the fluid density. We denote a scale for the (small) perturbation amplitude by ϵ, and write the variables as follows, where a prime denotes a perturbation quantity:

$$n = n_0 + \epsilon n', \quad \boldsymbol{u} = \epsilon \boldsymbol{u}', \quad p_e = p_{e0} + \epsilon p_e', \quad \boldsymbol{p} = \hat{\boldsymbol{k}} + \epsilon \boldsymbol{p}', \tag{3.1}$$

where $\hat{\boldsymbol{k}}$ is the unit vector in the vertically upwards 3−direction, and p_{e0} is the undisturbed excess pressure given by

$$\nabla p_{e0} = -n_0 v \Delta\rho g \hat{\boldsymbol{k}}$$

from (2.2).

Substitution of (3.1) into the governing equations and linearizing leads to the following set of equations, in which the components of $\boldsymbol{u}'$ have been taken to be (u', v', w'):

$$(2.1) \rightarrow \qquad \frac{\partial u'}{\partial x} + \frac{\partial v'}{\partial y} + \frac{\partial w'}{\partial z} = 0, \tag{3.2}$$

$$(2.2) \rightarrow \begin{cases} \rho \dfrac{\partial u'}{\partial t} = -\dfrac{\partial p_e'}{\partial x} + \mu \nabla^2 u', & (3.3) \\ \rho \dfrac{\partial v'}{\partial t} = -\dfrac{\partial p_e'}{\partial y} + \mu \nabla^2 v', & (3.4) \\ \rho \dfrac{\partial w'}{\partial t} = -\dfrac{\partial p_e'}{\partial z} - n' v \Delta\rho g + \mu \nabla^2 w', & (3.5) \end{cases}$$

$$(2.4), (2.6), (2.7) \rightarrow \frac{\partial n'}{\partial t} = -\operatorname{div}\left[n_0(\boldsymbol{u}' + V_c \boldsymbol{p}') + n' V_c \hat{\boldsymbol{k}} - D \nabla n'\right]. \tag{3.6}$$

If we write $\theta = \epsilon\theta'$, then (2.8) becomes

$$\boldsymbol{p}' = (\theta' \cos\phi, \ \theta' \sin\phi, \ 0) \tag{3.7}$$

and, with the notation $\boldsymbol{\omega} = \epsilon\boldsymbol{\omega}'$, $e_{ij} = \epsilon e_{ij}'$, (2.9) and (2.10) give

$$B^{-1}\theta' = -\xi \sin\phi + \eta \cos\phi,$$
$$0 = \xi \cos\phi + \eta \sin\phi,$$

where

$$\left.\begin{aligned} \xi &= \omega_1' - 2\alpha_0 e_{23}' = (1-\alpha_0)\frac{\partial w'}{\partial y} - (1+\alpha_0)\frac{\partial v'}{\partial z}, \\ \eta &= \omega_2' + 2\alpha_0 e_{13}' = -(1-\alpha_0)\frac{\partial w'}{\partial x} + (1+\alpha_0)\frac{\partial u'}{\partial z}. \end{aligned}\right\} \tag{3.8}$$

Hence

$$\tan\phi = -\xi/\eta, \quad \theta' = B(\xi^2 + \eta^2)^{\frac{1}{2}}$$

and

$$\boldsymbol{p}' = B(\eta, -\xi, 0). \tag{3.9}$$

Thus (3.6) can be rewritten as follows:

$$\frac{\partial n'}{\partial t} = V_c B n_0 \left(\frac{\partial \xi}{\partial y} - \frac{\partial \eta}{\partial x}\right) - V_c \frac{\partial n'}{\partial z} + D\nabla^2 n'. \tag{3.10}$$

The governing equations, (3.2)–(3.5) and (3.10) with (3.8), are linear differential equations with constant coefficients, so we can examine stability in terms of

individual Fourier modes. We therefore rewrite all perturbation quantities in the form (for example)

$$n'(x,y,z,t) = N\exp[\sigma t + \mathrm{i}(kx+ly+mz)],$$

substitute into the equations, and eliminate the amplitudes (N, etc.) to leave the following dispersion relation from which the growth rate σ can be determined in terms of the wavenumbers k, l, m:

$$(\sigma + \mathrm{i}mV_c + D\kappa^2)(\sigma+\nu\kappa^2) = \frac{\nu D\gamma^2}{\kappa^2}(\kappa^2-m^2)[(1-\alpha_0)\kappa^2+2\alpha_0 m^2], \tag{3.11}$$

where

$$\kappa^2 = k^2+l^2+m^2, \quad \nu = \mu/\rho$$

and

$$\gamma^2 = V_c Bn_0 vg\Delta\rho/\mu D. \tag{3.12}$$

Note that (*a*) γ has the dimensions of L^{-1} (like κ), suggesting that the critical or most rapidly growing disturbance will have wavenumber proportional to γ; (*b*) if there were no gyrotaxis, as in the model of Childress *et al.* (1975), B and hence γ would be zero; and (*c*) m is the vertical wavenumber, so $m = 0$ corresponds to a disturbance with no vertical variation.

Equation (3.11) is a quadratic equation for σ and can be easily solved. It is helpful, however, to examine simple special cases before writing down the general solution.

(i) *No gyrotaxis* When $\gamma = 0$ both solutions of (3.11) have negative real parts for all κ and therefore all disturbances decay: the suspension is unconditionally stable.

(ii) *No vertical variation* When $m = 0$ (and $\kappa^2 = k^2+l^2$) the roots of (3.11) can be written

$$\sigma = \tfrac{1}{2}\kappa^2\left[-(\nu+D)\pm\left\{(\nu+D)^2+4\nu D\left[\left(\frac{\gamma}{\kappa}\right)^2(1-\alpha_0)-1\right]\right\}^{\frac{1}{2}}\right]. \tag{3.13}$$

Thus one root is positive, and instability follows, if and only if κ is less than the critical value κ_c given by

$$\kappa_c = \gamma(1-\alpha_0)^{\frac{1}{2}}: \tag{3.14}$$

sufficiently long-wavelength disturbances will grow. Apart from the factor $(1-\alpha_0)^{\frac{1}{2}}$ this is the same result as that obtained by Kessler (1986*b*), who restricted his attention to spherical cells ($\alpha_0 = 0$) and horizontal, axisymmetric disturbances. Kessler, however, neglected fluid inertia (the σ-term in the second bracket of (3.11) was absent) and therefore concluded that σ increases as κ decreases (longer disturbances grow more rapidly). Inclusion of fluid inertia leads us to predict the existence of a most unstable disturbance: the positive solution of (3.13) is greatest when $\kappa = \kappa_m$, where

$$\left(\frac{\kappa_c}{\kappa_m}\right)^2 = 2+\frac{\nu+D}{(\nu D)^{\frac{1}{2}}}. \tag{3.15}$$

The positive value of σ is then

$$\sigma_m = \frac{\kappa_c^2\nu D}{(\nu^{\frac{1}{2}}+D^{\frac{1}{2}})^2}. \tag{3.16}$$

An estimate of the wavelength of the disturbance that will actually be observed experimentally is thus $2\pi/\kappa_m$: see table 1 for numerical values and §4 for further discussion.

(iii) *General solution* The root of (3.11) with greater real part is

$$\sigma = \tfrac{1}{2}\kappa^2 \left\{ -(\nu+D) - \frac{imV_c}{\kappa^2} + \left\{ \left(\nu + D + \frac{imV_c}{\kappa^2}\right)^2 - 4\nu D\left[1 - \left(\frac{\gamma}{\kappa}\right)^2 \left(1 - \frac{m^2}{\kappa^2}\right)\left(1 - \alpha_0 + 2\alpha_0 \frac{m^2}{\kappa^2}\right)\right]\right\}^{\frac{1}{2}} \right\}, \quad (3.17)$$

which can of course be computed for any given parameter values. First, however, suppose that $mV_c/\kappa^2 \ll \nu + D$, so that the imaginary terms in (3.17) can be neglected. Then, if we write

$$X = \frac{\kappa_c^2}{\kappa^2} > 0, \quad Y = \frac{m^2}{\kappa^2} > 0,$$

where κ_c^2 is given by (3.14), the root of (3.17) may be written

$$\sigma = \frac{\kappa_c^2}{2X}\{-(\nu+D) + [(\nu-D)^2 + 4\nu DX(1-Y)(1+\alpha' Y)]^{\frac{1}{2}}\}, \quad (3.18)$$

where

$$\alpha' = 2\alpha_0/(1-\alpha_0).$$

From (3.18) we shall draw three conclusions: (*a*) there are unstable disturbances with $m \neq 0$ and overall wavenumber κ greater than κ_c, as long as $\alpha_0 > \frac{1}{3}$; (*b*) there are unstable disturbances with $m \neq 0$ and *horizontal* wavenumber $\kappa_1 (= (k^2+l^2)^{\frac{1}{2}}) \geqslant \kappa_c$ (i.e. horizontal wavelength smaller than $\lambda_c = 2\pi/\kappa_c$) if $\alpha_0 > \frac{1}{2}$; (*c*) the most unstable disturbance has $m \neq 0$, and the maximum growth rate exceeds σ_m, if $\alpha_0 > \frac{1}{3}$.

There will be instability ($\sigma > 0$) if the square root in (3.18) exceeds $(\nu + D)$, and hence if

$$X(1-Y)(1+\alpha' Y) > 1; \quad (3.19)$$

and there are values of $X < 1$ ($\kappa > \kappa_c$) for which this is satisfied as long as

$$0 < Y < Y_c = \frac{\alpha' - 1}{\alpha'},$$

which is possible if $m \neq 0$ and $\alpha' > 1$, i.e. $\alpha_0 > \frac{1}{3}$. In that case the critical value of the total wavenumber κ is equal to $\kappa_c X_c^{-\frac{1}{2}}$, where X_c is given by equality in (3.19) when $Y = \frac{1}{2}Y_c$, i.e. $X_c = 1/\alpha_1$ where

$$\alpha_1 = \frac{(1+\alpha')^2}{4\alpha'} = \frac{(1+\alpha_0)^2}{8\alpha_0(1-\alpha_0)}. \quad (3.20)$$

Now $\alpha_1 > 1$ if $\alpha_0 \neq \frac{1}{3}$, so the critical value of κ is greater than κ_c, which is conclusion (*a*). It can be shown similarly that there are unstable disturbances with horizontal wavenumber $\kappa_1 \geqslant \kappa_c$ and non-zero m if $\alpha' > 2$, i.e. $\alpha_0 > \frac{1}{2}$ (result *b*). Moreover, when $\alpha' > 1$, the maximum value of σ occurs when $\partial\sigma/\partial Y = \partial\sigma/\partial X = 0$, i.e. from (3.18),

$$Y = \tfrac{1}{2}Y_c, \quad \alpha_1 X = (\kappa_c/\kappa_m)^2, \quad (3.21)$$

where κ_m is given by (3.15). Thus $m \neq 0$, $\kappa = \alpha_1^{\frac{1}{2}}\kappa_m$, and the corresponding maximum growth rate is $\alpha_1 \sigma_m$, given by (3,16); this exceeds σ_m if $\alpha' \neq 1$, i.e. $\alpha_0 \neq \frac{1}{3}$; this is result (*c*). We conclude that, as long as the mV_c/κ^2 term is negligible, the suspension is more unstable to three- than to two-dimensional disturbances if the cells are sufficiently elongated.

The physical mechanism for this unusual result may be thought of as follows. As

α_0 increases to one, the particles become more rod-like and, in their vertical orientation, their response to horizontal shear diminishes to zero. Thus in the limit $\alpha_0 = 1$, the fluid is stable to two-dimensional disturbances, as implied by the expression (3.14) for κ_c. However if $m > 0$ (for example when there are distant horizontal boundaries, as in (iv) below), then there is vertical shear in the flow pattern, which tends to orientate the elongated particles away from the vertical. In this manner, gyrotaxis can render the suspension unstable. The most unstable vertical mode is established by a balance between gyrotaxis and the stabilizing effect of diffusion D. For a given initial state, as m increases, so does the gyrotactic response of the particles. But, diffusion also becomes more dominant as m increases, until it overcomes gyrotaxis at a sufficiently large value of m.

A suitable scale for mV_c/κ^2 is V_c/γ, and in practice this is about 0.1ν (see table 1 and §4) , so neglect of this term is justified. If it is retained in (3.17), but assumed small, the above prediction of maximum growth rate is reduced by a factor of approximately

$$1-\frac{m^2V_c^2}{\kappa_c^4}\frac{\nu+(\nu D)^{\frac{1}{2}}+D}{\nu D(\nu^{\frac{1}{2}}+D^{\frac{1}{2}})^2}.$$

Moreover, however large mV_c/κ^2 is, the presence of the imaginary term in (3.17) cannot stabilize an otherwise unstable disturbance. To see this, write (3.17) as

$$\frac{2\sigma}{\kappa^2} = (\nu+D)\{-1-\mathrm{i}r+[(1+\mathrm{i}r)^2+S]^{\frac{1}{2}}\},$$

where $S > 0$ for a disturbance to be unstable when $r = 0$; then $\mathrm{Re}\,(\sigma) > 0$ if $\mathrm{Re}\,[(1+\mathrm{i}r)^2+S]^{\frac{1}{2}} > 1$ for $S > 0$. Now set $[(1+\mathrm{i}r)^2+S]^{\frac{1}{2}} = x+\mathrm{i}y$, eliminate y, and solve the resulting quadratic equation for x^2; the positive root can be readily shown to exceed 1. Thus the critical wavenumber $\alpha_1^{\frac{1}{2}}\kappa_c$ is unchanged by the presence of the mV_c/κ^2 term. Furthermore the 'principle of exchange of stabilities' holds for this example, because $\mathrm{Im}\,(\sigma) = 0$ when $\mathrm{Re}\,(\sigma) = 0$ (i.e. when $S = 0$).

(iv) *Finite depth* The objective of our theoretical work is to explain the formation of bioconvection patterns observed experimentally (Kessler 1985*b*, 1986*a*, etc.). However, experiments are inevitably done in chambers of finite depth, and this puts a lower bound on the possible values of the vertical wavenumber m, even for nearly spherical cells for which the most unstable disturbance was predicted to be two-dimensional for the case of infinite depth. Ignoring the fact that a uniform, upwards-swimming suspension does not satisfy realistic boundary conditions in a chamber of finite depth, say H, let us use the above theory to examine the instability for the case of spherical cells ($\alpha_0 = 0$) when $m \geqslant m_0 = 2\pi/H$.

In this case the inequality (3.19) shows that instability occurs if

$$\kappa_c^2(\kappa^2-m^2) > \kappa^4.$$

Thus the critical values of the horizontal wavenumber $\kappa_1 = (\kappa^2-m^2)^{\frac{1}{2}}$ are given by

$$(\kappa_1^2+m_0^2)^2 = \kappa_c^2\kappa_1^2,$$

i.e. for instability κ_1 must lie between the two positive roots of this equation:

$$\kappa_1 = \tfrac{1}{2}\kappa_c\left\{1\pm\left(1-\frac{4m_0^2}{\kappa_c^2}\right)^{\frac{1}{2}}\right\}. \tag{3.22}$$

It can be seen that no real, positive value of κ_1^2, or in other words no horizontally periodic disturbance of the form assumed here, exists if $m_0^2 > \frac{1}{4}\kappa_c^2$. Since for spherical

cells $\kappa_c = \gamma$ (equation (3.14)), we can rearrange this inequality to conclude that there is no instability unless the *gyrotactic Rayleigh number* $R = \gamma^2 H^2$ exceeds the critical value of $16\pi^2 \approx 158$. It can also be shown from (3.18) that, when $R > 16\pi^2$, the most rapidly growing disturbance has horizontal wavenumber given by

$$\frac{\kappa_{1m}^2}{\kappa_c^2} = -\frac{2\nu D}{(\nu - D)^2} - \frac{m^2}{\kappa_c^2} + \frac{\nu + D}{\nu - D}\left\{\frac{\nu D}{(\nu - D)^2} + \frac{m^2}{\kappa_c^2}\right\}^{\frac{1}{2}}. \tag{3.23}$$

Decreasing the layer depth from infinity (increasing m_0 from zero) causes κ_{1m} to increase to a maximum value of m_0 when m_0 takes its maximum value (for instability) of $\frac{1}{2}\kappa_c$. Thus the horizontal wavelength of the most unstable disturbance is predicted to decrease with depth, from $2\pi/\kappa_m$ (equation (3.15)) to $4\pi/\kappa_c$. However, quantitative reliance should not be placed on these results because the basic state does not satisfy the boundary conditions of zero cell flux across the horizontal boundaries. This is discussed further below.

4. Discussion

The main conclusions of the above analysis are as follows.

(i) An infinite uniform suspension of gyrotactic micro-organisms is unstable in the absence of concentration (and hence density) stratification, unlike a suspension of vertically swimming cells as analysed by Childress *et al.* (1975).

(ii) There is instability only for sufficiently long disturbances, with wavenumber κ less than a critical value, as found by Kessler (1986*b*).

(iii) There is a most rapidly growing disturbance with a non-zero value of κ; this conclusion differs from that of Kessler (1986*b*) who ignored fluid inertia and found the maximum growth rate to occur for $\kappa = 0$.

(iv) If the cells are sufficiently elongated ($\alpha_0 > \frac{1}{3}$), both the critical and the most unstable disturbances are three-dimensional (with non-zero vertical wavenumber), whereas they are two-dimensional if the cells are approximately spherical.

(v) If the chamber containing the suspension has finite depth, instability develops only if the 'gyrotactic Rayleigh number' R exceeds a critical value, equal to $16\pi^2$ if the cells are spherical, and the most unstable horizontal wavelength decreases as layer depth decreases.

Of the above conclusions it is (iii), the prediction of a most unstable disturbance, that is most amenable to quantitative testing against observation, since the most unstable disturbance is expected to be the one that first manifests itself at an amplitude large enough to be seen. In this section we present parameter values appropriate to past experiments (e.g. Kessler 1986*a*, *b*), and show that the predicted wavelength of the most unstable disturbance is somewhat larger than the wavelengths of observed steady-state convection patterns. We also give further discussion of some of the idealizations in the present model and the extent to which they need to be amended in order to conform more closely to experiment.

In table 1 the values of the 'input' parameters are given, many of them taken from the corresponding table of Kessler (1986*b*). Two of the quantities (marked with an asterisk) can only be roughly estimated and might be considerably in error: possible values of diffusivity D are discussed in §2 above, while the centre-of-mass offset h has been assessed from the rate at which the orientations of isolated individuals change when they are not initially vertical. The ratio of major-to-minor axes of the cell, α_0, is easily measured from photographs at suitable magnification, and the value

Symbol	Definition	Range	Value for *C. nivalis*
ρ	Water density	1.0	1.0 g cm^{-3}
$\rho+\Delta\rho$	Cell density	1.01–1.10	1.05 g cm^{-3}
d	Average cell diameter	4×10^{-4}–4×10^{-3}	10^{-3} cm
v	Cell volume	3×10^{-11}–3×10^{-8}	5×10^{-10} cm^3
h^*	Centre of gravity offset	0–0.05d	10^{-5} cm
α_0	Cell eccentricity parameter (equation (2.11))	0–0.5	0.31
$\alpha_\perp$	Viscous torque parameter	6–9	6.8
V_c	Swimming speed	0–2×10^{-2}	10^{-2} cm s^{-1}
n_0	Background number density	0–10^7	10^6 cells cm^{-3}
D^*	Cell diffusivity	5×10^{-5}–10^{-3}	10^{-4} cm^2 s^{-1}
μ ($\nu=\mu/\rho$)	Suspension viscosity	10^{-2}	10^{-2} g cm^{-1} s^{-1} (cm^2 s^{-1})
g	Gravitational acceleration	10^3	10^3 cm s^{-2}

Table 1. Values of the 'input' parameters of the model. The ranges are derived from observation and from the literature (see Kessler 1986*b*); the values in the last column apply approximately to *Chlamydomonas nivalis*, often used in experiments (Kessler 1984, 1986*b*). Quantities marked * have not been directly measured and are merely plausible inferences.

quoted in the final column was measured on several individuals of *Chlamydomonas nivalis*. It can be seen to be only a little less than the critical value ($\frac{1}{3}$) for the appearance of three-dimensional instability; indeed, certain individuals are more elongated than this ($\alpha_0 = 0.5$). If experiments were performed with a population consisting only of elongated cells (e.g. *Dunaliella parva*), it should be possible to check conclusion (iv) above (as long as the initial stirring motions were damped out quickly: see below). The viscous torque parameter $\alpha_\perp$ can be calculated from formulae originally given by Jeffrey (1922) and quoted in the Appendix of P & K: it takes the value 6 for a sphere and 8 when $\alpha_0 = 0.5$.

In table 2 are given the derived quantities relevant to this paper. Some of these are required in order to assess the validity of assumptions made in the analysis, and others represent predictions, to be checked against experiment. In the former category are: $n_0 v$, correctly assumed to be $\ll 1$; cell spacing d_0, supposed to be small compared with lengthscales of the flow field, such as λ_c and λ_m given in table 2; the sedimentation velocity V_S, calculated from Stokes's formula for a sphere, which has to be small compared with the cell swimming speed V_c.

The main prediction is the wavelength of the most unstable disturbance; given that $\alpha_0 < \frac{1}{3}$, this disturbance will be two-dimensional ($m = 0$) and its wavelength is $\lambda_m = 2\pi/\kappa_m$, predicted to be close to 9 mm. If the planform of the convection is that of rolls, i.e. the down-moving regions of large cell concentration are parallel sheets, with $k = \kappa_m$, $l = 0$ say, then their spacing should be about 9 mm. On the other hand, if the planform is square, with $k = l = 2^{-\frac{1}{2}}\kappa_m$, then the side of the square should be $2^{\frac{1}{2}}\lambda_m \approx 13$ mm.

The main difficulty in comparing the predicted wavelength with observation is the fact that the almost steady bioconvection patterns that are set up some time after the initiation of the experiment have a significantly smaller wavelength than the disturbances observed initially (Kessler 1986*a*, figures 14, 15). This is because the ultimate flow is inevitably nonlinear: as the convection develops, the downflow regions, or plumes, become stronger and therefore attract cells more rapidly, so that after some time the majority of the cells are in the plumes, and the assumption of a

small perturbation has broken down. Eventually, as Kessler (1986*b*) has shown in a simple model for axisymmetric plumes, a singularity will develop if the region from which each plume attracts cells is too wide, which leads to a prediction of maximum, steady-state plume spacing of (in our notation) $2^{\frac{3}{2}}/\gamma \approx 1$ mm. This is much closer to the observed steady-state spacing of 1 to 3 mm (Kessler 1985*b*, 1986*a*) than the above prediction of 9–13 mm. A nonlinear, time-dependent theory should be developed, in order to predict both the planform of the convection and the eventual plume spacing.

There are only a few observations of the development of the patterns with time shown by Kessler (1986*a*). His figure 14 shows biconvection patterns, in 6 mm deep suspensions viewed from above, (*a*) using *Chloromonas rosae*, where the concentrated regions form sheets or curtains whose spacing decreases from about 6 mm to about 2 mm as the time t after stirring was stopped increases from 60 s to 100 s; and (*b*) using *Chlamydomonas nivalis*, where the concentrated regions are plumes whose spacing decreases from about 2.7 mm to about 1.2 mm as t increases from 40 s to 1 min 40 s. Kessler's figure 15 gives a side view of a 2.5 cm deep suspension of *C. nivalis*, and again the spacing between concentrated regions decreases from about 3.9 mm and above to about 2.3 mm as t goes from 15 s to 105 s. These trends are consistent with the theories, and although none of the published patterns has a wavelength as large as the predicted values of 9–13 mm, some recent observations suggest that the wavelengths of early disturbances may be that large. A systematic experimental study of time-dependent bioconvection remains to be carried out.

The early stages of plume formation, revealed by figure 15 of Kessler (1986*a*), are, however, difficult to interpret. The suspension is initially well-stirred, and the initial sites of cell concentration, although largely aligned vertically, show horizontal streaks and patchiness as well. While this could be the manifestation of a three-dimensional instability, as analysed above for elongated cells, it seems more likely that the phenomenon results chiefly from the nucleation of streamers by fluid motions which remain after stirring and which cause gyrotaxis *ab initio*. (Note that Childress 1981, p. 135 also refers to the early patterns being 'formed during the decay of the swirl'.) Experiments in which such motions have been quickly damped out by a regularly spaced array of horizontal cylinders have produced only vertical spontaneous streamers, which is consistent both with the geometrical constraints and with the fact that the cells were probably not very elongated.

A further potential reason for the difference between the predicted and observed wavelengths is poor estimation of some of the relevant parameters, in particular h and D. However, κ_{m} is approximately proportional to $h^{-\frac{1}{2}}D^{-\frac{1}{4}}$ (assuming $D^{\frac{1}{2}}$ is much less than $\nu^{\frac{1}{2}}$). To decrease λ_{m} by a factor of 3 would require decreasing h by a factor of 9 or D by a factor of 81; the latter seems to be beyond possibility, and the former would make h so small that stable gyrotaxis could occur only with extremely weak flows (the cells are predicted to tumble if the horizontal vorticity exceeds approximately B^{-1}: Kessler 1986*a*). Thus inaccurate parameter estimation is probably not important.

Another aspect of the experiments of Kessler (1985*b*, 1986*a*) is that they were conducted in fluid layers of finite depth H, mainly in the range 2–11 mm as well as in deep chambers with $H = 25$ mm and above. With $\gamma = 29\ \mathrm{cm}^{-1}$ (table 2), these depths correspond to values of the Rayleigh number $R = \gamma^2 H^2$ in the range 34–1020, and then over 5200, greater than the critical value for spherical cells of 158, if $H > 4.3$ mm. (The somewhat more complicated calculation for non-spherical cells with $\alpha_0 = \frac{1}{3}$ and $\alpha' = 1$ gives a slightly smaller critical value of R of $9\sqrt{3}\pi^2 \approx 154$.) The

Symbol and definition	Meaning	Value
$n_0 v$	Volume concentration	5×10^{-4}
$d_0 = n_0^{-\frac{1}{3}}$	Cell spacing	10^{-2} cm
$V_s = gv\Delta\rho/3\pi d\mu$	Sedimentation velocity	3×10^{-4} cm s^{-1}
$B = \mu\alpha_\perp/2h\rho g$	Gyrotactic orientation parameter (equation (2.12))	3.4 s
$\gamma = (V_c B n_0 v g \Delta\rho/\mu D)^{\frac{1}{2}}$	Wavenumber scale (equation (3.12))	29 cm^{-1}
$\kappa_c = \gamma(1-\alpha_0)^{\frac{1}{2}}$	Critical wavenumber for $m = 0$ (equation (3.14))	24 cm^{-1}
$\lambda_c = 2\pi/\kappa_c$	Critical wavelength	0.26 cm
$\kappa_m = \kappa_c(\nu D)^{\frac{1}{4}}/(\nu^{\frac{1}{2}} + D^{\frac{1}{2}})$	Wavenumber of fastest-growing disturbance (equation (3.15))	7.0 cm^{-1}
$\lambda_m = 2\pi/\kappa_m$	Wavelength of fastest-growing disturbance	0.9 cm
$\sigma_m = \kappa_c^2 \nu D/(\nu^{\frac{1}{2}} + D^{\frac{1}{2}})^2$	Growth rate of fastest-growing disturbance (equation (3.16))	0.004 s^{-1}

TABLE 2. Derived quantities: definition and estimated values for *C. nivalis*

lower bound on the vertical wavenumber m is predicted to alter the most unstable horizontal wavenumber κ_{1m} (equation (3.23)). This increases from κ_m (given by (3.15)) to m_0 when $m_0 = \frac{1}{2}\kappa_c$, and hence for spherical cells the horizontal scale (λ_{1m}) of the most unstable disturbance is predicted to decrease from 7.5 mm to 4.3 mm as H decreases from infinity to 4.3 mm. This prediction represents a further interesting contrast with experimental results, because figure 10 of Kessler (1985*b*) demonstrates that the horizontal wavelength of (quasi-) steady-state convection patterns *increases* as depth is decreased. Measurement from the figure gives $\lambda \approx 2$ mm for $H = 11$ mm, $\lambda \approx 4$ mm for $H = 2$ mm. The reason for the difference may well again lie in the difference between the dynamics governing the steady state and those determining the onset of convection.

However, the present theory is not in any case expected to be valid for very shallow layers. As already indicated in §3, the basic state of a uniform suspension of upward-swimming cells does not satisfy the boundary condition of zero cell flux across the horizontal boundaries, at $z = 0$ and $z = -H$, say. The appropriate steady state is one of exponential height dependence,

$$n_0(z) = n_0(0) \exp(V_c z/D), \tag{4.1}$$

as analysed for non-gyrotactic cells by Childress *et al.* (1975) (and for gyrotactic cells by the present authors in a forthcoming paper). In an experiment the suspension is initially well mixed, with uniform concentration, but with more-or-less random fluid motions, which remain from the stirring, still present. What happens next depends on the relative magnitudes of three different timescales: the time for the stirring motions to decay, T_d, the time for the upward self-concentration leading to (4.1) to develop significantly, T_s, and the time for the growth of organized convective disturbances, T_m. If T_d is much less than both T_s and T_m, the stirring motions can be ignored except as a source of the perturbations from which instability grows. In that case, if $T_s \ll T_m$, an upwardly concentrated distribution will be set up before disturbances grow, and the present theory is inapplicable. On the other hand, if $T_m \ll T_s$, convection of the form analysed here will develop throughout the chamber, except probably in thin layers near the boundaries, before the cell distribution changes much. The appropriate scale for T_s is H/V_c, the time for a cell to swim all the way up the chamber, which for $H = 5$ mm or 15 mm is 50 s or 150 s respectively.

The final approach to the distribution (4.1) will in fact take the longer diffusive

time, $H^2/4\pi^2 D$, which has the values 10^3 s and 4×10^3 s for the two depths; however, significant departures from n_0 = constant will occur on the shorter timescale. The relevant value of T_m is σ_m^{-1} (see table 2), or about 15 s, which is significantly less than T_s, for the depths considered here. The eddy decay time T_d for a turbulent flow is of order equal to the eddy size H divided by a typical stirring velocity (Batchelor 1953). Thus the decay becomes more gradual as the velocities fall, but T_d will still be much less than T_s (and, to a lesser extent, T_m) when the stirring velocity has fallen below typical convective velocities, which are significantly greater than V_c; Kessler (1986*a*) quotes 0.25 cm s^{-1} as a typical value (the present linear theory does not permit prediction of convective velocities). The conclusion is that the present theory is approximately valid for the depths considered.

Financial support from the National Science Foundation (grant No. INT 85-13696) and the Science and Engineering Research Council is gratefully acknowledged.

REFERENCES

BATCHELOR, G. K. 1953 *The Theory of Homogeneous Turbulence*. Cambridge University Press.

BATCHELOR, G. K. 1970 The stress system in a suspension of force-free particles. *J. Fluid Mech.* **41**, 545–570.

CHILDRESS, S. 1981 *Mechanics of Swimming and Flying*. Cambridge University Press.

CHILDRESS, S., LEVANDOWSKY, M. & SPIEGEL, E. A. 1975 Pattern formation in a suspension of swimming micro-organisms. *J. Fluid Mech.* **69**, 595–613.

HINCH, E. J. 1972 Note on the symmetries of certain material tensors for a particle in Stokes flow. *J. Fluid Mech.* **54**, 423–425.

JEFFREY, G. B. 1922 The motion of ellipsoidal particles immersed in a viscous fluid. *Proc. R. Soc. Lond.* A **102**, 161–179.

KESSLER, J. O. 1984 Gyrotactic buoyant convection and spontaneous pattern formation in algal cell cultures. In *Nonequilibrium Cooperative Phenomena in Physics and Related Fields* (ed. M. G. Velarde), pp. 241–248. Plenum.

KESSLER, J. O. 1985*a* Hydrodynamic focusing of motile algal cells. *Nature* **313**, 218–220.

KESSLER, J. O. 1985*b* Cooperative and concentrative phenomena of swimming micro-organisms. *Contemp. Phys.* **26**, 147–166.

KESSLER, J. O. 1986*a* The external dynamics of swimming micro-organisms. In *Progress in Phycological Research*, vol. 4 (ed. F. E. Round), pp. 257–307. Bristol: Biopress.

KESSLER, J. O. 1986*b* Individual and collective dynamics of swimming cells. *J. Fluid Mech.* **173**, 191–205.

LEVANDOWSKY, M., CHILDRESS, S., SPIEGEL, E. A. & HUTNER, S. H. 1975 A mathematical model of pattern formation by swimming micro-organisms. *J. Protozool.* **22**, 296–306.

LOEFFER, J. B. & MEFFERD, R. B. 1952 Concerning pattern formation by free-swimming micro-organisms. *Am. Naturalist* **86**, 325–329.

PEDLEY, T. J. & KESSLER, J. O. 1987 The orientation of spheroidal micro-organisms swimming in a flow field. *Proc. R. Soc. Lond.* B **231**, 47–70.

PLATT, J. R. 1961 "Bioconvection patterns" in cultures of free-swimming micro-organisms. *Science* **133**, 1766–1767.

PLESSET, M. S. & WINET, H. 1974 Bioconvection patterns in swimming microorganism cultures as an example of Rayleigh–Taylor instability. *Nature* **248**, 441–443.

ROBERTS, A. M. 1970 Motion of spermatozoa in fluid streams. *Nature* **228**, 375–376.

RÜFFER, V. & NULTSCH, W. 1985 High-speed cinematographic analysis of the movement of *Chlamydomonas*. *Cell Motility* **5**, 251–263.

WINET, H., BERNSTEIN, G. S. & HEAD, J. 1984 Observations on the response of human spermatozoa to gravity, boundaries and fluid shear. *J. Reprod. Fert.* **70**, 511–523.

WINET, H. & JAHN, T. L. 1972 On the origin of bioconvective fluid instabilities in *Tetrahymena* culture systems. *Biorheol.* **9**, 87–94.